Shaking Table Tests on Gravel Slopes Reinforced by Concrete Canvas

Guangya Ding, Ph.D

College of Civil Engineering and Architecture, Wenzhou University, Chashan University Town, Wenzhou, China. E-mail: gyding321@163.com

Lin Zhou, Master's student

College of Civil Engineering and Architecture, Wenzhou University, Chashan University Town, Wenzhou, China. E-mail: 1315193949@qq.com

Jun Wang*, Ph.D, Corresponding author

College of Civil Engineering and Architecture, Wenzhou University, Chashan University Town, Wenzhou, China

Key Laboratory of Engineering and Technology for Soft Soil Foundation and Tideland Reclamation, Wenzhou University, Zhejiang, Wenzhou, China

Telephone: +86 577 886689687; Fax: +86 577 886689611; E-mail: junwang8006@hotmail.com

Ying Xu, Ph.D

School of Civil Engineering and Architecture, Anhui University of Science and Technology, Taifeng Street, Huainan, China. E-mail: 1026984957@qq.com

Xueyu Geng, Ph.D

Geotechnical Engineering School of Engineering, University of Warwick, Coventry, UK.

E-mail: Xueyu.Geng@warwick.ac.uk

Xiaobin Li, Ph.D

College of Civil Engineering and Architecture, Wenzhou University, Chashan University Town, Wenzhou, China. E-mail: 00151022@wzu.edu.cn

Shaking Table Tests on Gravel Slopes Reinforced by Concrete Canvas

Abstract: The behaviour and performance of different reinforced slopes during earthquake loading were investigated through a series of shaking table tests. Concrete-canvas and composite reinforcement (geogrid attached to concrete-canvas) were proposed for reinforcing slopes. By considering the effects of different reinforcement methods, the seismic responses of the reinforced slopes were analysed, along with the accelerations, crest settlements, and lateral displacements. The failure patterns of different model slopes were compared using white coral sand marks placed at designated elevations to monitor the internal slide of the reinforced slopes. Both the concrete-canvas and composite reinforcement could increase the safety distance, which ranged from the slide-out point to the back of the model box. The composite reinforcement decreased the volume of the landslide and increased the failure surface angle as a result of the larger global stiffness in the reinforced zone. These results indicate that the recently developed concrete canvas has a better effect on restricting the slope deformation during seismic loading than the nonwoven geotextile reinforcement, and that the use of composite reinforcement could improve the seismic resistance of slopes.

Keywords: Geosynthetics, slope, concrete canvas, reinforcement, shaking table

1 Introduction

In seismic active regions, earthquake induced collapses constitute a part of devastating natural disasters. However, reinforced slopes and retaining walls can be used to reduce the damage. These should show satisfactory seismic performance and cost effectiveness. Reinforcement materials can be characterized as inextensible and extensible ones. Extensible geosynthetic reinforcement is often used in

slopes and can enhance the performance of slopes by decreasing deformation. Building steep reinforced slopes in less space has been an interesting topic to geotechnical engineers over the years.

Geosynthetic reinforced walls have been widely used in the past few decades given their good performance in terms of the ductility of structures (EI-Emam and Bathurst 2007; Murali Krishna and Madhavi Latha 2007; Panah et al., 2015; Yazdandoust 2017; Song et al., 2018; Huang 2019; Fan et al., 2020; Xu et al., 2020). To examine the influence of reinforcement parameters (i.e., the length, stiffness, and vertical spacing) on wall design, El-Emam and Bathurst (2007) performed model tests with rigid facing slabs. Furthermore, Panah et al. (2015) conducted massive experiments on 80-cm-high walls reinforced by polymers. Those researchers also discussed the influence of the reinforcement material arrangement on the model response. However, compared with reinforced walls, studies on the dynamic responses of reinforced slopes with gentle slopes are relatively limited, particularly studies on gravel slopes (Lin et al., 2015; Edinçliler and Toksoy 2016; Srilatha et al., 2016; Xu and Yang 2019; Wang et al., 2019). Meanwhile, for reinforced slopes, most studies have focused on the reinforcing effect of geotextile. For example, Huang et al. (2011) conducted shaking table tests on geotextile reinforced slopes with a stepwise intensified sine load. The results showed that the acceleration amplification factor is a function of the base frequency and that a change from an amplification state to a de-amplification state occurred when the input ground acceleration reached a certain level. Srilatha et al. (2013) investigated the influence of seismic frequency on the dynamic responses of geotextile reinforced slopes. They found that the displacement increased proportionately with the seismic frequency, whereas frequency had little effect on the acceleration amplifications. Furthermore, Srilatha et al. (2016) investigated the effects of different reinforcement materials (geotextiles and geogrids) on the response of a model slope. Their results showed that a geotextile-reinforced slope better reduced lateral deformation compared to a geogrid-reinforced slope, and that varying the reinforcement quantity had no effect on the acceleration amplification. As the strength between the geotextile and backfill interface is relatively low, particularly in multi-layered interfaces, sliding problems of reinforced soils are often caused by the weakening of the interaction between the reinforcement and the soil. Fortunately, a recently developed

concrete canvas has demonstrated good tensile strength and bond force, which could significantly increase the friction between the backfill and reinforcement. Therefore, it would be worthwhile to investigate the seismic performance of the concrete canvas in reinforced slopes.

This study evaluates the performance of a proposed concrete-canvas reinforcement and composite reinforcement (geogrid attached to concrete-canvas) in reinforcing slopes. By considering the effects of different reinforcement methods, the behaviour and performance of the reinforced slopes during seismic excitation were analysed, along with the accelerations, crest settlements, and lateral displacements. The failure patterns of different model slopes were compared by monitoring the residual length of white coral sand marks placed at designated elevations. Furthermore, the safety distance from the slide-out point to the back of the model box was calculated under the conditions of concrete-canvas and composite reinforcements.

2 Shaking table tests

2.1 Shaking table

To evaluate the performance of the concrete-canvas reinforcement, shaking table tests were performed. The shaking table loading platform had dimensions of 3.6 m × 1.3 m, with a maximum bearing capacity of 50 kN. The shaking table could be controlled within the acceleration range of 0-1 *g* and the frequency range of 0-10 Hz with a 100-mm amplitude. To clearly observe the slope deformation, a model box fabricated from rigid, transparent Plexiglas sheet was used. The model box had a rectangular cross section with internal dimensions of 2.1 m × 1.0 m and 1.1-m depth. A 50 mm thick foam sheet was placed in the model to reduce the reflection of waves (Panah et al. 2015; Yazdandoust 2017).

2.2 Similitude rules

To accurately simulate the dynamic response of a reinforced slope, appropriate similitude rules are required for the test. In this study, the similitude laws presented by Iai (1989) were used; these laws are widely adopted, being employed in many 1-*g* model tests. In accordance with the bearing capacity of the

shaking table, the similarity ratio to the geometric size was determined to be 1:6. The geometric size, mass density, and acceleration were taken as control variables. Other variables could be deduced from the Buckingham π theory. Details of the scaling factors are listed in Table 1, where λ is the prototype-to-model scale.

2.4 Materials

2.4.1 Backfill materials

Uniformly graded gravel samples with a maximum particle diameter of 1.3 cm were employed as backfill materials. The physical properties of the backfill soil are listed in Table 2.

2.4.2 Reinforcement materials

The following three different types of reinforcement materials were used: a nonwoven geotextile, geogrid, and concrete canvas. The concrete canvas had a 3-D fabric structure, which was composed of polyethylene and polypropylene filled with a specific dry concrete mix. Polyvinyl chloride backing was attached to its bottom surface. The details of the concrete canvas structure are shown in Fig. 1. In practical engineering applications, it is only necessary to immerse it into water, which will generate a hydration reaction between the water and concrete layer until a certain hardness is formed and its bottom surface will bond to backfill as an integrity, which will significantly increase the interface strength between the backfill and the concrete canvas. To prevent the loss of dry concrete, a mixed polyvinyl chloride (PVC) backing was utilized. Thus, before watering, the polyvinyl chloride (PVC) backing will need to be torn off, and then, the concrete canvas and backfill will bond with integrity. The geosynthetic part of the concrete canvas has good tensile strength, which satisfies a basic condition for use as a reinforcement material. In addition, the concrete canvas has good durability, which means it will have a long period of service and will decrease the maintenance costs for the reinforced slope. The properties of the concrete canvas are given in Table 3.

2.5 Instruments

Accelerometers, displacement meters, and earth pressure sensors were used in this study. The full-scale acceleration range of the analogue voltage output accelerometers was 2 g along the *x*, *y*, and *z* axes. The displacement meters were used to measure the slope crest settlement.

3 Model construction and test procedures

3.1 Model construction

To effectively control the compaction, a 10-kg mass was dropped from a height of 500 mm onto a steel base plate of 200 mm × 200 mm square. Reinforcement materials were placed at the interfaces of the compacted layers at elevations of 400, 520, and 640 mm, respectively. During the compaction process, five displacement meters were positioned along the slope crest at distances of 0, 110, 220, 330, and 400 mm from the edge of the slope to measure the vertical settlement. Three accelerometers were installed in the soil at elevations of 200, 400, and 600 mm from the bottom of the slope, with one additional accelerometer, A0, being installed on the model surface to measure the base acceleration. The instrumentation arrangement is displayed in Fig. 1. To observe the internal sliding of each slope, white coral sands were deposited at elevations of 200, 400, 500, and 600 mm during construction of the model slope.

3.2 Reinforcement arrangements

To evaluate the efficiency of various reinforcement, shaking table tests were performed on reinforced slopes. As noted by Liu et al. (2014), the failures start with the sliding and rolling down of gravels on the surface of the slope near the crest, and thus, in this study the reinforcement should be placed within the top zone of the model. Five reinforcement layer arrangements were used: an unreinforced slope (Model 1), a geotextile-reinforced slope (Model 2), a concrete-canvas-reinforced slope (Model 3), a composite-reinforced slope (Model 4) and a two-layer-concrete-canvas-reinforced slope (Model 5). As above mentioned, the bond force of bottom surface of concrete canvas can provide great friction between the backfill and the concrete canvas, whereas the top surface of concrete canvas is relatively smooth compared to the bottom surface. Therefore, in order to increase the friction between

the backfill and the top surface of concrete canvas geogrid was attached to the top surface of concrete canvas. This reinforcement method was referred as composite reinforcement. The reinforcement arrangements are presented in Fig. 1. The reinforcement was kept at a distance of 150 mm from the slope surface.

3.3 Test procedures

To investigate the influence of different reinforcement methods, on the dynamic responses of reinforced slopes, five model slopes were constructed during the tests. Considering the scale factors presented in Table 1, frequencies in the range of 3.3 to 10 Hz could be applied to the slope. Here, 4 Hz was chosen as the frequency to be used in the model. Note that rolling and sliding failures are the major slope failures occurring on a gravel slope during an earthquake. The resonant frequency is a vital factor in model tests, and it can be calculated from the shear wave velocity. The shear wave velocity equation was given as follows (Hardin and Richart, 1963):

$$V_s = [13.788 - (6.488 \times e)] \times (\sigma_v')^{\frac{1}{4}}, \quad (1)$$

where V_s is the shear wave velocity, e is the soil void ratio, and σ_v' is the mean effective confining pressure. Further, the natural frequency of model slope can be calculated from its shear wave velocity (Chen at al., 2006):

$$f_n = \frac{V_s}{4\sqrt{Hh}}, \quad (2)$$

in which f_n and H are the natural frequency and elevation of the model slope, respectively. h is the thickness of landslide body. The calculation results indicated that in this test the applied motion frequency was less than the fundamental frequency of the model slope; hence, the model was not subjected to resonance.

4 Effects of different reinforcement methods

4.1 Acceleration responses

The acceleration responses during shaking were recorded. The distributions of the peak ground acceleration (PGA) amplification factor (normalised by the input PGA) and the mitigation ratio of the PGA amplification factor are shown in Fig. 2, in which UR represents the unreinforced slope and CR represents the composite reinforced slope. The PGA amplification factor distribution patterns for the unreinforced and composite-reinforced slope are identical. However, the PGA amplification of composite-reinforced slope is smaller than that of unreinforced-slope, which is due to that composite reinforcement has a stronger constraint on soils and could accelerate the dissipation of seismic energy when the seismic waves travel upward. The PGA amplification decreased with increased input amplitude, because larger deformation induces greater hysteretic material damping. Based on the mitigation ratio of the PGA amplification factor, the reinforcing effect was more effective at the top of the slope. This indicates that it is reasonable to place reinforcement materials in the top zone of the slope. Furthermore, at 600-m elevation, the attenuation rates were 9%, 8%, and 3% at 0.7, 0.5, and 0.3 *g*, respectively. These results show that the employed composite reinforcement could have a better reinforcing effect when subjected to stronger shaking (exceeding 0.5 *g*).

4.2 Crest settlements

Fig. 3 shows the effects of different reinforcement methods on the crest settlement of gravel slopes at the L4 point. The crest settlements for Model 1 were much larger than other models and the measured values of Model 1 were not shown in Fig. 3. With the earthquake intensity increased, the crest settlement also increased as shown in Fig. 3. The measured crest settlements of Model 1 at a distance of 330 mm were 0.41, 9.3, and 73 mm at 0.3, 0.5, and 0.7 *g*, respectively. The corresponding settlements for Model 2 were reduced to 0.27, 1.62, and 4.95 mm at the selected accelerations, whereas the corresponding settlements for Model 3 were reduced to 0.25, 1.09, and 2.21 mm. These test results show that a concrete canvas more effectively reduces the slope crest settlement than geotextile reinforcement. Furthermore, compared to Model 3, the maximum crest settlement was smaller in Model 4, and this phenomenon was more prominent at higher acceleration. This result proves that use of composite reinforcement is feasible. Note that the differential settlements between the various slopes were very minor at 0.3 *g*, which implies

that the induced deformation had not reached the threshold level at which the mitigating effects of the composite reinforcement and concrete-canvas reinforcement become effective.

Next, to investigate the advantage of composite reinforcement versus geotextile reinforcement, the crest settlement attenuation rates were calculated through normalisation against the crest settlement of the geotextile-reinforced slope. Fig. 3 also shows the variation of the crest settlement attenuation rates between different models for three kinds of accelerations at measurement point L4. As the earthquake intensity increased, the crest settlement attenuation rates also increased. This indicates that the reinforcing effect was more significant at a stronger intensity. Compared to the case of geotextile reinforcement, the crest settlement was reduced by 11%, 57%, and 66% when the concrete canvas was employed, under input motions of 0.3, 0.5, and 0.7 *g*, respectively. When the composite reinforcement was used, the crest settlement was reduced by 19%, 64%, and 73% when subjected to the same corresponding input motions. Thus, the composite reinforcement was more effective than the individual concrete-canvas reinforcement. For both concrete-canvas-reinforced and composite-reinforced slopes, the crest settlement rates exhibited significant improvement at an input motion of 0.5 *g*.

The typical crest settlement variations in accordance with the loading cycle number for different models at point L5 are shown in Fig. 4. Comparison of Models 1 and 4 shows that the composite reinforcement could reduce the maximum crest settlement by approximately 75% under an input motion of 0.7 *g*. After shaking for 12 cycles, the crest settlement on the geotextile-reinforced slope continued to increase, reaching 63 mm at the end of the input motion of 0.7 *g*. However, the crest settlement on Model 4 could be well controlled by the applied composite reinforcement and could be restricted at 32 mm until termination of the 0.7 *g* input motion. Therefore, the composite reinforcement can be regarded as the more effective prevention method with regard to potential sliding failure of gravel slopes.

4.3 Horizontal displacements

To study the mitigating effect of the composite reinforcement on the horizontal displacement of slopes, the horizontal displacements recorded for 0.7 *g* base shaking are shown in Fig. 5. In this test, the displacement toward to the direction of model back is defined as negative, conversely, the displacement

towards to the direction of slope surface is defined as positive. As apparent from this figure, the horizontal displacements of Models 1–3 were negative at elevations exceeding 400 mm, and the horizontal displacement increased with higher elevation. These results indicate that seismically induced gravel rolling or sliding failures occurred at the tops of the slopes, and that stronger seismic responses were found at higher elevations; this is consistent with the observations of Liu et al. (2014). To some extent, the horizontal displacement curve shapes for Models 4 and 5 differ from those of Models 1–3. In particular, the horizontal displacement for Model 4 suddenly increased to approximately 80 mm at an elevation of approximately 415 mm, as reflected in the curve. It should be noted that the reinforcement materials were installed above 400-mm elevation. These results show that composite reinforcement increases the strength and integrity of the reinforced zone, which caused the major slide-out point shift from the crest of the slope to the bottom of the reinforced zone. Then a larger horizontal displacement (sudden change point) at the elevation of around 400 mm was observed in Model 4. The appearance of a sudden change point for Model 4, for which the composite reinforcement was employed, implied that composite reinforcement had a better reinforcing effect in restricting gravel rolling than geotextile reinforcement. Comparing the horizontal displacements for Models 4 and 5, that for the latter was smaller than that for Model 4 at the top of the slope, which implies that the reinforcing effect of the composite reinforcement is better than that of 1-layer reinforcement and slightly worse than that of 2-layer-concrete-canvas reinforcement. It is likely that the reinforcing effect obtained for Model 4 reached the ultimate bearing capacity attainable by 1-layer composite reinforcement. The distribution of the horizontal displacement attenuation rate (normalised by the horizontal displacement of the unreinforced slope) vs. the elevations of Models 1–3, for which the horizontal displacement curve shapes were similar, is also shown in Fig. 6. The horizontal displacement attenuation rates increased with elevation, indicating improved reinforcement at higher elevation.

4.4 Failure patterns

Fig. 7 shows the failure patterns of all slopes subjected to the 0.7 *g* input motion. The efficiency of the various reinforcement methods with regard to the failure patterns is discussed individually below. A sliding body that developed from the slope crest is apparent for Models 1–3. This failure pattern differs from that of Model 4, for which the sliding body developed from the bottom of the reinforced zone, and from that of Model 5, for which the sliding phenomenon was invisible for the case of 0.7-*g* input motion. This clearly indicates that composite reinforcement and 2-layer-cancrete-canvas reinforcement increase the strength of the reinforced zone compared to other reinforcement methods.

The distance from the slide-out point to the back of the model box was defined as the safety distance. A comparison of the safety distances of Models 1 and 2 reveals that the geotextiles used in Model 2 increased the safety distance by approximately 54%. A comparison of Models 1 and 3 shows that the concrete canvas could increase the safety distance by approximately 61%, which means that the concrete canvas used in Model 3 can better restrict gravel falls than geotextile reinforcement used in Model 2. Figs. 20 (c) and (d) illustrate that Model 4, for which the composite reinforcement was used, exhibited far superior performance as regards increasing the safety distance for the same shaking compared to Model 3, in which a concrete canvas was used. These results clearly show that Model 4 is the most efficient measure for controlling the safety distance with 1-layer reinforcement. The superior reinforcing effect obtained for Model 4 is attributed to the greater friction at the upper surface of the reinforcement materials.

The failure surface angles with the vertical line varying from 45° to 60° for different slopes are shown in Fig. 7. Note that an increase in the global stiffness of the reinforced zone generated a larger failure surface angle. Furthermore, when the global stiffness of the reinforced zone reached a threshold level, the slide-out point transferred from the crest of the slope to the bottom of the reinforced zone, as shown for Models 4. For Model 5 subjected to 0.7-*g* input motion, the obvious failure surface angle was invisible; however, a slight decline marked by the white coral sands was apparent in areas C and D, as shown in Fig. 7 (e). In contrast, the white coral sands maintained stability in areas A and B. This shows that the slide-point position for Model 5 was similar to that for Model 4. From the above phenomena, it

could be concluded that the slide-out point of reinforced slope will change when the reinforcing effect reaches a critical level.

The lengths of the residual white coral sand deposits placed at the 200-, 400-, 500-, and 600-mm elevations were measured in order to monitor the internal sliding of the slope, as shown in Fig. 7. From the measured values, the slope failure process can be progressive and follows the "surface-to-interior" model. The different residual lengths of the white coral sand deposits for Models 1–4 were very minor at lower elevation but increased dramatically at upper elevation, as shown in Fig. 7. The effects of different reinforcement methods on the control of the internal sliding of the slopes were quantified by the increment rates of the residual lengths of the white coral sand deposits, as shown in Fig. 8. This increment rate was calculated based on normalisation by the length of the residual white coral sand deposit of the unreinforced slope. The increment rates of the residual lengths of the white coral sand deposits at the 200-mm elevation were 6%, 8%, and 9% for Models 2–4, respectively, which indicates that the bottom 2/7th zone of the slope was relatively stable during the earthquake and the reinforcement was ineffective at the bottom of the slope. However, the increment rates of the residual lengths of the white coral sand deposits at the 600-mm elevation were 20%, 31%, and 36% for Models 2–4, respectively. A superior reinforcing effect as regards restriction of the internal sliding of the slope was observed in the top 4/7th zones of the slopes.

5 Conclusions

A series of shaking table tests were performed to investigate the efficacy of various reinforcement methods to enhance slope stability. The improvements provided by these reinforcement methods were determined by comparing the acceleration responses, crest settlements, horizontal displacements, and failure patterns. The following major conclusions were drawn.

(1) Compared to geotextile reinforcement, the maximum crest settlement can be reduced by 40% and 59% by employing concrete canvas and composite reinforcement, respectively, when subjected to 0.7-*g* input motion. For input motion is larger than 0.5 *g*, the concrete canvas and composite

reinforcements can have a satisfactory reinforcing effect. However, since the reinforcement materials and the layout of the reinforcement used in this study are unusual, it is not fit for widespread application in actual slope engineering.

(2) With increasing elevation, the reinforcing effect is improved. When the reinforcing effect reaches a threshold level, the slide-out point shifts from the crest of the slope to the bottom of the reinforced zone. The reinforcing effect of the composite reinforcement is larger than that of all 1-layer reinforcements and reaches the threshold level.

(3) Compared to an unreinforced slope, composite reinforcement can increase the safety distance by approximately 67%. With increasing global stiffness of the reinforced zone, the failure surface angle is increased. The slope fails in the “high-to-low” mode and the sliding zone gradually expands inward.

It has to be noted that these findings were obtained for the geometrical configuration chosen in the experiments. Hence, the conclusions should not be extrapolated to field scale models. Also, the results reported may be useful for developing and validating numerical procedures in analysed the seismic behaviour of the composite reinforcement.

Acknowledgement

This study was supported by the National Key R&D Program of China (2016YFC0800200), the Zhejiang Provincial Natural Science Foundation of China (LY18E080027), the National Natural Science Foundation of China (51578425 and 51978534), and the Zhejiang Provincial Science and Technology Planning Project (2015C31026).

References

Chen, L.L., Gao, M.A., Qian, S.G. 2006. New theory of distinguishing slope stability -inherent frequency discrimination. Rock Soil Mech. 27, 1219–1222.

El-Emam, M.M., Bathurst, R.J. 2007. Influence of reinforcement parameters on the seismic response of reduced-scale reinforced soil retaining walls. Geotext. Geomembr. 25, 33–49.

Edinçliler, A., Toksoy, Y.S. 2016. Physical model study of the seismic performance of highway embankments with and without geotextile. J. Earthq. Tsunami 11, 81–98.

Fan, C., Liu, H.B., Cao, J.Z., Ling, H.I. 2020. Responses of reinforced soil retaining walls subjected to horizontal and vertical seismic loadings. Soil Dyn. Earthq. Eng. 129, 105969.

Huang, C.C., Horng, J.C., Chang, W.J., Chiou, J.S., Chen, C.H. 2011. Dynamic behavior of reinforced walls – horizontal displacement response. Geotext. Geomembr. 29, 257–267.

Huang, C.C. 2019. Seismic responses of vertical-faced wrap-around reinforced soil walls. Geosynth. Int. 26(2), 146–163.

Hardin, B., Richart, F. 1963. Elastic wave velocities in granular soils. J Soil Mech. Found. Div. (ASCE) 89, 33–66.

Iai, S., 1989. Similitude for shaking table tests on soil-structure-fluid model in 1g gravitational field. Soils Found. 29 (1), 105–118.

Lin, Y.L., Leng, W.M., Yang, G.L., Li, L., Yang, J.S. 2015. Seismic response of embankment slopes with different reinforcing measures in shaking table tests. Nat. Hazards 76, 791–810.

Liu, J., Liu, F., Kong, X., Yu, L. 2014. Large-scale shaking table model tests of aseismic measures for concrete faced rock-fill dams. Soil Dyn. Earthq. Eng.61-62, 152–163.

Murali Krishna, A., Madhavi Latha, G. 2007. Seismic response of wrap-faced reinforced soil-retaining wall models using shaking table tests. Geosynth. Int. 14, 355–364.

Panah, A.K., Yazdi, M., Ghalandarzadeh, A. 2015. Shaking table tests on soil retaining walls reinforced by polymeric strips. Geotext. Geomembr. 43, 148–161.

Song, F., Liu, H.B., Hu, H.B., Xe, Y.L. 2018. Centrifuge tests of geocell-reinforced retaining walls at limit equilibrium. J. Geotech. Geoenviron. Eng. 144(3), 04018005.

Srilatha, N., Madhavi Latha G., Puttappa, C.G. 2013. Effect of frequency on seismic response of reinforced soil slopes in shaking table tests. Geotext. Geomembr. 36, 27–32.

Srilatha, N., Madhavi Latha, G.M., Puttappa, C.G. 2016. Seismic response of soil slopes in shaking table tests: effect of type and quantity of reinforcement. Int. J. Geosynth. and Ground Eng. 2(4), 33.

Wang, Y.Q., Liu, K., Li, X., Ren, Q.B., Li, L.L., Zhuang, Z.H., Li, M.C. 2019. Experimental and upper-bound study of the influence of soilbag tail length on the reinforcement effect in soil slopes. Geotext. Geomembr. 47, 610–617.

Xu, P., Hatami, K., Jiang, G.L. 2020. Study on seismic stability and performance of reinforced soil walls using shaking table tests. Geotext. Geomembr. 48, 82–97.

Xu, J.S., Yang, X.L. 2019. Seismic stability of 3D soil slope reinforced by geosynthetic with nonlinear failure criterion. Soil Dyn. Earthq. Eng. 118, 86–97.

Yazdandoust, M. 2017. Investigation on the seismic performance of steel-strip reinforced-soil retaining walls using shaking table test. Soil Dyn. Earthq. Eng. 97, 216–232.

Figures

Tables

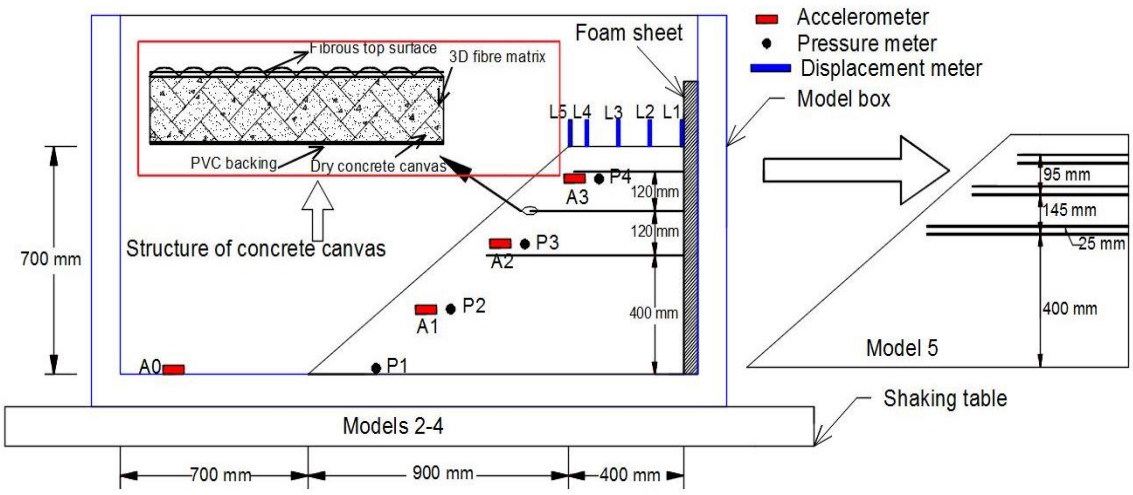

Fig. 1 Schematic diagrams of reinforced model slope with sensors

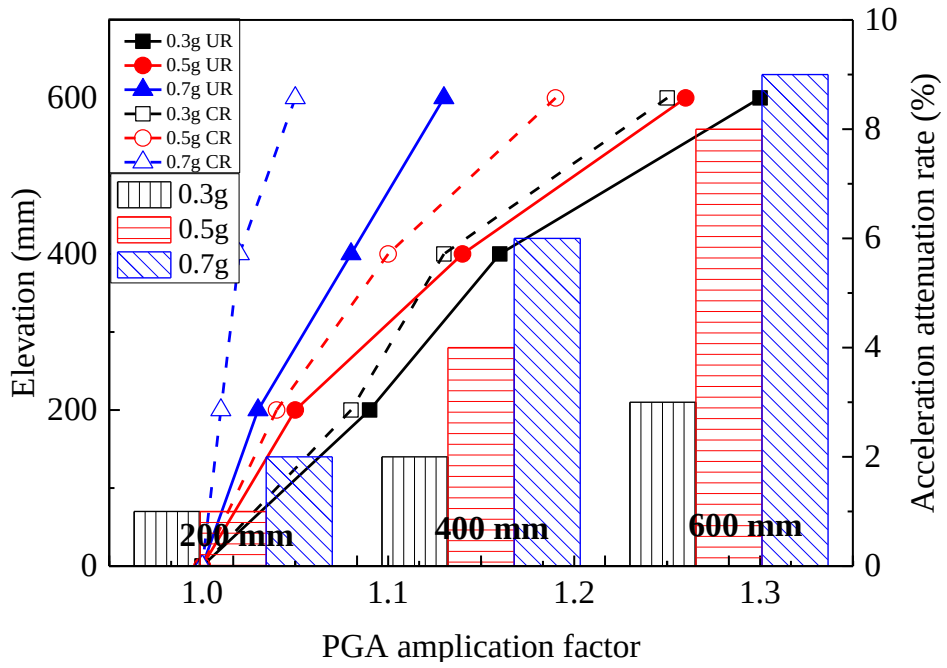

Fig. 2 PGA amplification factor and its mitigation ratio for different input motions

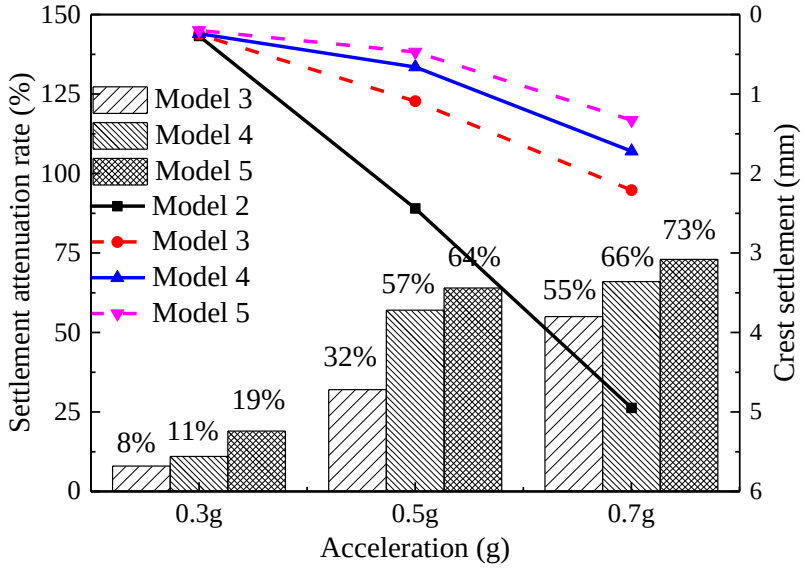

414

415 **Fig. 3** Crest settlements and its attenuation rates for different input motions

416

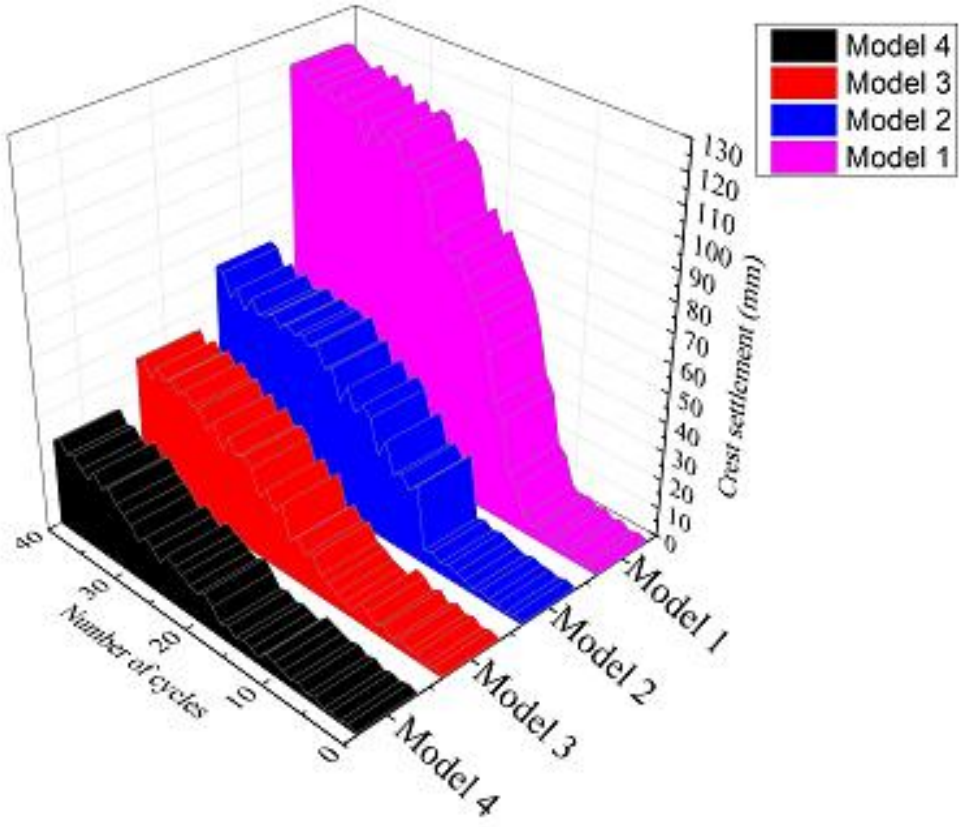

417

418 **Fig. 4** Typical crest settlement variations with the number of cycles for different models

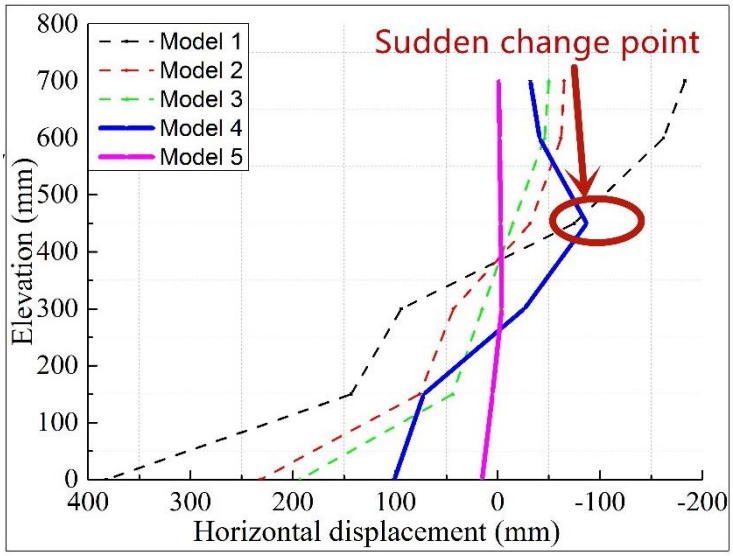

419

420 **Fig. 5** Elevation versus horizontal displacement for different models

421

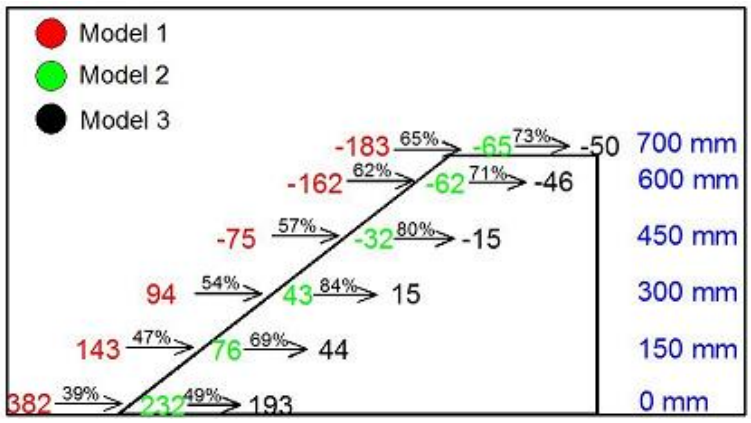

422

423 **Fig. 6** Horizontal displacement attenuation rate for different models

424

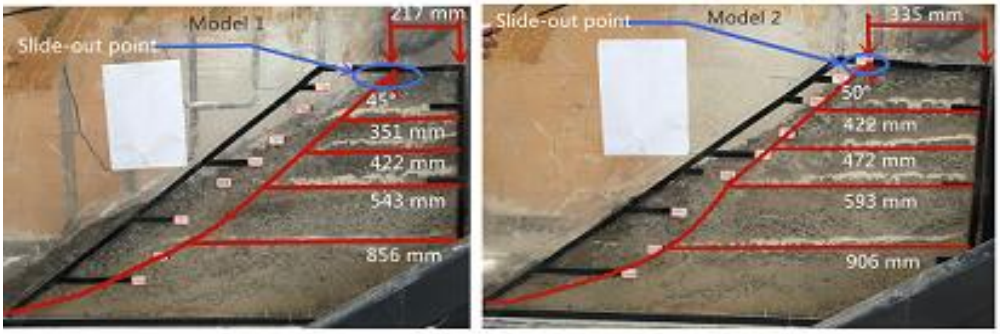

(a) (b)

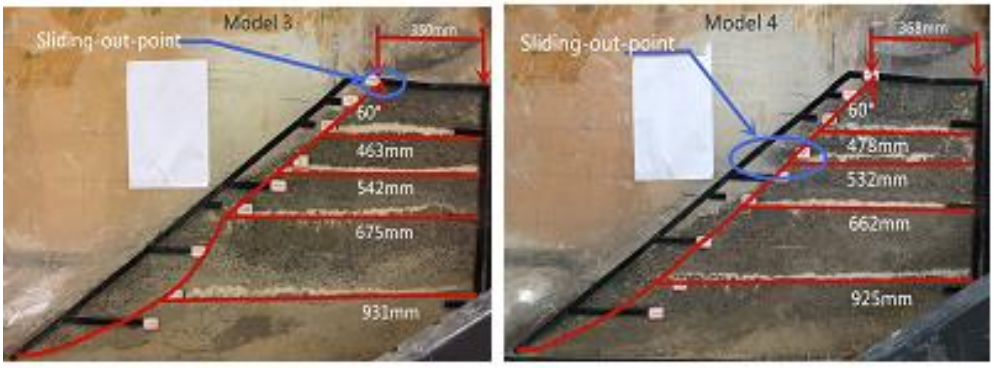

(c) (d)

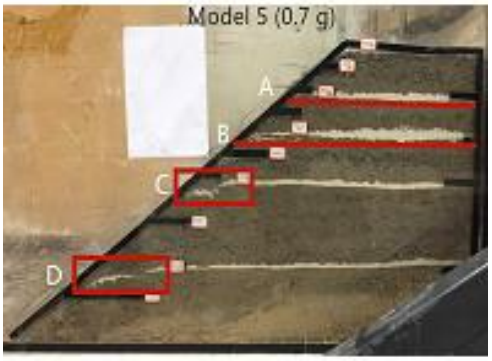

(e)

Fig. 7 Failure patterns: (a)–(e) Models 1–5

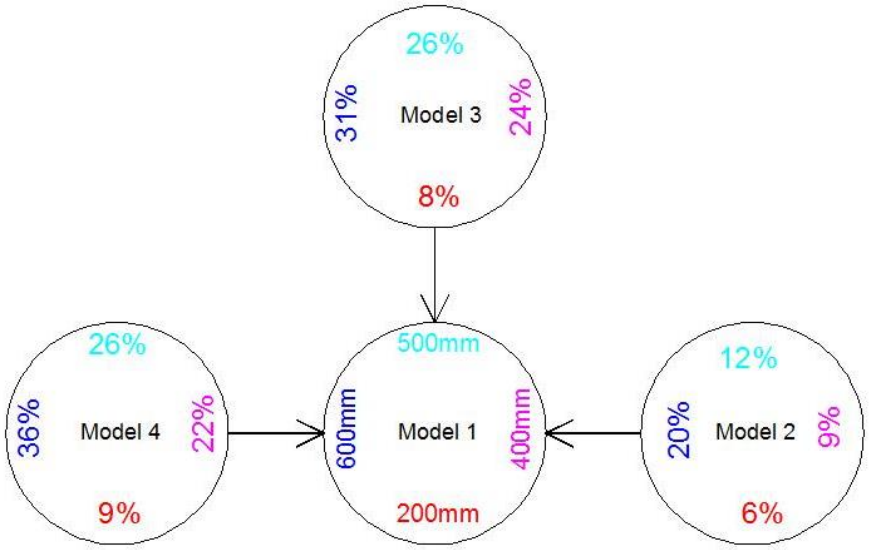

433

434 **Fig. 8** Increment rate of residual lengths of white coral sand deposits

435

436

Table 1 Scale factors for shaking table test model

Description	Parameter	Scale factor (Prototype/Model)	Scaling in test	Remarks
Geometric length	l	λ	6	Control variable
Acceleration	*a*	1	1	Control variable
Density	ρ	1	1	Control variable
Displacement	*s*	λ	6	
Dynamic time	*t*	$\lambda^{3/4}$	3.8	
Frequency	ω	$\lambda^{-3/4}$	0.3	
Stress	σ	λ	6	
Strain	ξ	$\lambda^{1/2}$	2.5	

Table 2 Physical properties of the backfill soil

D_{60} (mm)	D_{50} (mm)	D_{30} (mm)	D_{10} (mm)	C_c	C_u	Φ (°)	G_s
8.7	7.8	6.1	3.3	1.3	2.6	45.0	2.5

451

452 Table 3 Properties of the concrete canvas

Parameter	Value
Ultimate tensile strength (kN/m)	25.2
Break point strain (%)	25.4
Tensile strength at 2% strain (kN/m)	7.1
Tensile strength at 5% strain (kN/m)	13.2
Thickness (mm)	10.0
Mass per unit area (kg/m^2)	18.0
Initial setting time (min)	>120.0
Final setting time (min)	<240.0

453